Aerodynamic Analysis of an Airfoil With Leading Edge Pitting Erosion

Yan Wang
Key Laboratory of Mechanics on Environment and Disaster in Western China, Ministry of Education, Lanzhou University, Lanzhou 730000, China;
School of Energy and Power Engineering, Lanzhou University of Technology, Lanzhou 730050, China

Ruifeng Hu
Research Center for Applied Mechanics, School of Mechano-Electronic Engineering, Xidian University, Xi'an 710126, China

Xiaojing Zheng
Key Laboratory of Mechanics on Environment and Disaster in Western China, Ministry of Education, Lanzhou University, Lanzhou 730000, China;
Research Center for Applied Mechanics, School of Mechano-Electronic Engineering, Xidian University, Xi'an 710126, China
e-mail: xjzheng@lzu.edu.cn

Leading edge erosion is a considerable threat to wind turbine performance and blade maintenance, and it is very imperative to accurately predict the influence of various degrees of erosion on wind turbine performance. In the present study, an attempt to investigate the effects of leading edge erosion on the aerodynamics of wind turbine airfoil is undertaken by using computational fluid dynamics (CFD) method. A new pitting erosion model is proposed and semicircle cavities were used to represent the erosion pits in the simulation. Two-dimensional incompressible Reynolds-averaged Navier–Stokes equation and shear stress transport (SST) k–ω turbulence model are adopted to compute the aerodynamics of a S809 airfoil with leading edge pitting erosions, where the influences of pits depth, densities, distribution area, and locations are considered. The results indicate that pitting erosion has remarkably undesirable influences on the aerodynamic performance of the airfoil, and the critical pits depth, density, and distribution area degrade the airfoil aerodynamic performance mostly were obtained. In addition, the dominant parameters are determined by the correlation coefficient path analysis method, results showed that all parameters have non-negligible effects on the aerodynamics of S809 airfoil, and the Reynolds number is of the most important, followed by pits density, pits depth, and pits distribution area. Meanwhile, the direct and indirect effects of these factors are analyzed, and it is found that the indirect effects are very small and the parameters can be considered to be independent with each other. [DOI: 10.1115/1.4037380]

Keywords: pitting erosion, aerodynamic performance, path-coefficient analysis, S809 airfoil

1 Introduction

Wind power generation has developed significantly during last decades for its clean and renewable characteristics. Driven by the requirements in energy capture and wind turbine technology, the scope and size of modern wind turbine have grown considerably and single turbine power can reach a capacity of 8–10 MW with rotor diameters in excess of 160 m [1]. However, various harmful environmental conditions, such as rain drops, sand, hailstone, and other abrasive airborne particles, could be great threat to the mechanical integrity of wind turbine blade, especially at the leading edge [2]. Leading edge erosion has been stated as one of the challenges and main issues for manufacturers and operators of wind turbines in many articles and reports [3,4]. The erosion usually arises from the formation of small pits near the leading edge, which develops gradually and combines into gouges [5]. If without repairing in time, the gouges will continuously grow in size and depth, and delamination could be finally formed. Thus, the overall leading edge erosion process of a wind turbine blade can be classified into pits, gouges, and final delamination [6,7]. Some blade maintenance engineers found that there was a great deal of pits and holes on the surface of offshore wind turbine blades, which may grow to cracks after only 2 years of operation [8]. Ehrmann et al. [9] stated that an energy loss of 20% or more was caused by leading edge erosion after installing for about 3 years, and about 6% of the wind turbine maintenance was related to leading edge erosion or defect of blades. In China, blade erosion has become a significant problem, e.g., it was reported that 50% of wind turbine blades were with the problem of leading edge erosion, gel coat damage, or cracks on the blade surfaces after 3–5 years of operation [10]. Leading edge erosion can induce flow separation and transition to turbulence, no matter severe or slight, which impose unfavorable effects on wind turbine performance and would finally result in power losses [11]. Therefore, to deep understand the influence of leading edge erosion on wind turbine performance quantitatively and take steps to mitigate the adverse influence are important for wind turbine blades maintenance and wind farm operators' management [12,13].

It has been documented [4,14–16] that leading edge erosion can adversely affect the aerodynamic characteristics of an airfoil, and result in lift loss and drag increase, finally affecting the energy harvesting characteristics of a wind turbine. Sareen et al. [6] demonstrated that there would be a 6–500% drag increase and 3–5% to 25% annual energy loss due to slight or heavy erosions by wind tunnel experiments. Gharali and Johnson [17] found that leading edge cavity erosion could induce average (maximum) lift decreases between 17% and 34% (48–76%) of S809 airfoil with various erosion extents through numerically simulation. Wang et al. [18] indicated that cavity erosion at the leading edge can give rise to the emergence of leading separation bubble and flow separation at the tailing edge, which play great roles on lift decrease and drag increase of the airfoil; however, the aerodynamic coefficients do not change much when the erosion length reaches to certain value at given erosion thickness.

Although the detrimental effects of erosion on wind turbine performance have been investigated in some studies for different kinds of erosion types, we still know little about the pitting erosion. In the present study, computational fluid dynamics (CFD) method was adopted to study the effects of leading edge erosion on aerodynamic performances of a S809 airfoil at the initial stage of erosion, i.e., pitting erosion. The erosion was characterized by pits size, density, and area. The purpose is to find the influential rules of this

Contributed by the Solar Energy Division of ASME for publication in the Journal of Solar Energy Engineering: Including Wind Energy and Building Energy Conservation. Manuscript received February 8, 2017; final manuscript received June 15, 2017; published online August 31, 2017. Assoc. Editor: Yves Gagnon.

Fig. 1 Photograph of the leading edge with pitting erosion. A photograph from the company of wind turbine equipment maintenance [21].

kind of leading erosion and obtain the relationship between the influence factors, and finally find out the most dominant one. The paper is arranged as follows: The pitting erosion model is introduced and described in Sec. 2. The computational method and its validation are introduced in Sec. 3. The results and analysis are given in Sec. 4. The final conclusions are drawn in Sec. 5.

2 Pitting Erosion Model

Reports and photographs of Vestas turbines and 3M by field observation have showed that the first stage of blade erosion is in the form of small pinholes of missing paint distributed across the leading edge of blade surface [6,19,20]. A close look of wind turbine blade with pitting erosion is shown in Fig. 1 [21]. It has been reported that the size and depth of the missing paint pinholes are generally small and always distributed in the first 10% of the chord length [6,21]. In the experimental study of Sareen et al. [6] and Chinmay [5], the pit's size (diameter) was set to be 0.51 mm and spanned over the 10%c of the upper surface and 13%c of the lower surface at the leading edge of the wind turbine blade. Gaudern [19] described that pits depth is always ranging from 0.1 to 1.2 mm with a coverage ranging from 3%c to 8%c of a wind turbine blade. Therefore, in order to study the effects of pits depths, densities, and coverage area on the performance of airfoil in detail, a pitting erosion model is proposed in the present study, and semicircle cavities are adopted to represent the erosion pits, as shown in Fig. 2(*a*). In this model, the surface of the airfoil is covered by semicircle cavities with radiuses ranging from 0.1 to 2.5 mm (Table 1), l indicates the distance between two erosion pits as a quantity representing the pits distribution density, and h is the erosion depth. The pitting erosion area is located at the leading edge of the airfoil, as illustrated in Fig. 2(*b*), in which x is the chordwise erosion length.

Table 1 Pits depth considered in the simulation

Unit	Pits depth (h)								
mm	0.1	0.2	0.3	0.5	0.8	1	1.5	2	2.5
h/c	0.0001	0.0002	0.0003	0.0005	0.0008	0.001	0.0015	0.002	0.0025

Note: h/c is the ratio of pits depth and chord length of the airfoil.

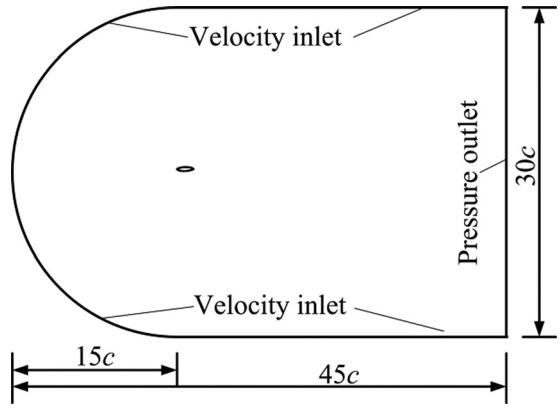

Fig. 3 Computational domain

3 Computational Method

Two-dimensional incompressible Reynolds-averaged Navier–Stokes equations were numerically solved by the commercial CFD software ANSYS FLUENT 15.0 [22]. Segregated solver and implicit and SIMPLEC algorithm were adopted for coupling the momentum and pressure equations. Second-order upwind differencing scheme was chosen for spatial discretization because of its good accuracy and stability. The details of solver setup can be inferred the software ANSYS [22].

3.1 Computational Setup

3.1.1 Computational Domain. Proper computational domain is important in obtaining more accurate results and eliminating the effects of far-field boundary. In our previous work, simulation experiments were conducted and found that 15c from boundary to airfoil is a distance large enough for eliminating the boundary reflections [18]. Thus, in this study, the computational domain is made up of a semicircle with a radius of 15c and a rectangular with a length of 30c, as shown in Fig. 3. The airfoil is placed at the center of the semicircle.

3.1.2 Grid Generation. The quality of the computational grids is crucial for the accuracy of CFD simulations, especially to describe the flow in the pitting cavities. Therefore, to examine the grid sensitivity inside the pits on the computational results, several grid generation schemes in the semicircle cavities are discussed later.

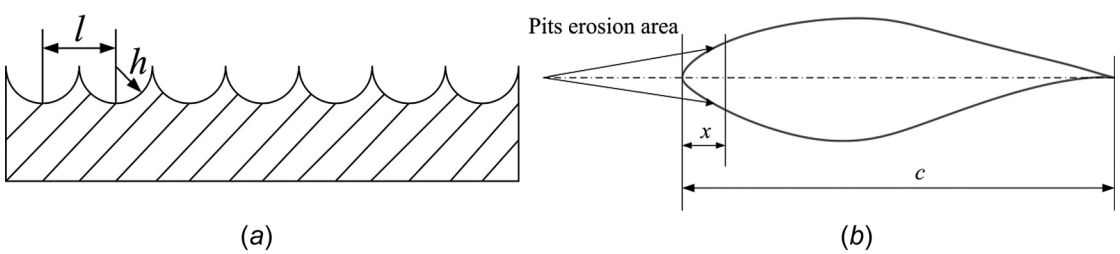

Fig. 2 The pitting erosion model. (*a*) The equivalent erosion pits and its distribution. (*b*) Location of pitting erosion area on an S809 airfoil.

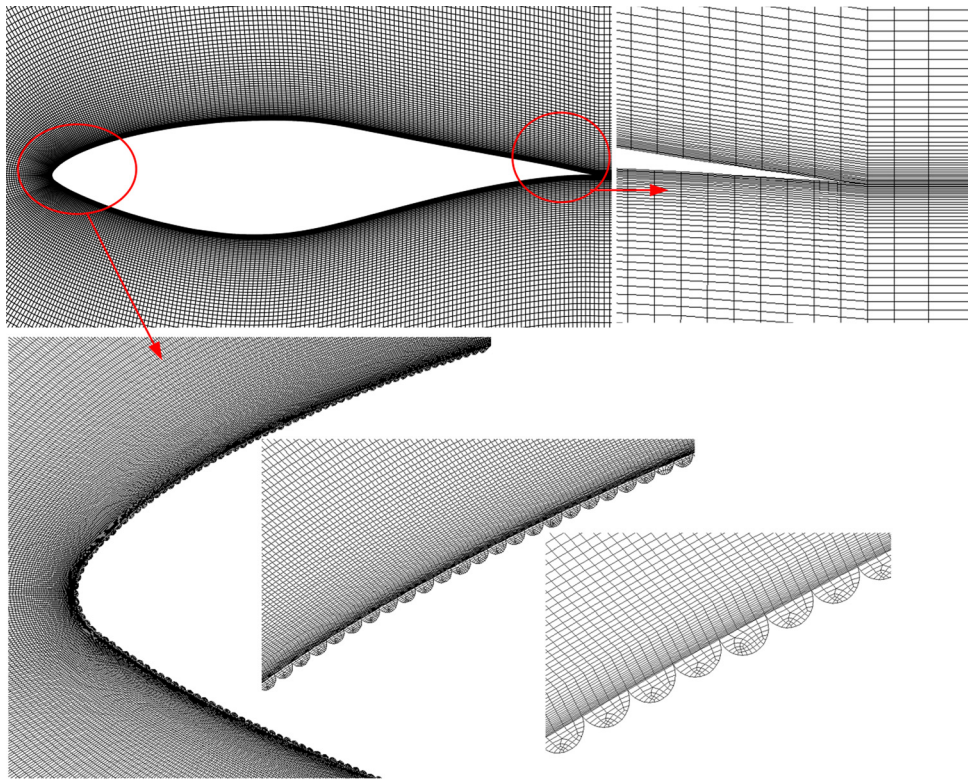

Fig. 4 Global grid and local grid near the leading edge, trailing edge, and the pits

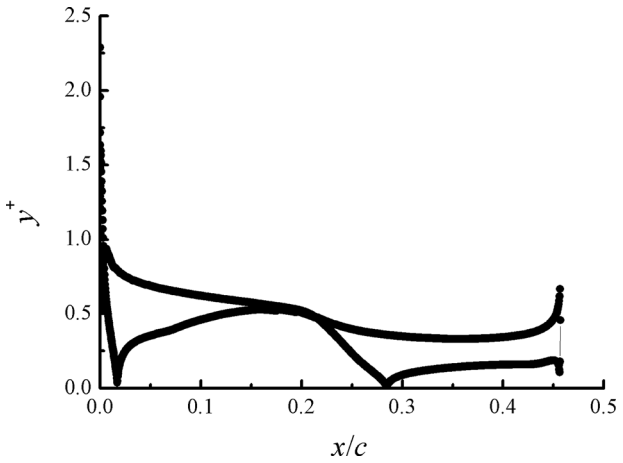

Fig. 5 The value of *y* plus adjacent to the airfoil

Figure 4 shows the computational grid used in the present study, which was composed of two regions, a typical C-type structured quadrilateral grid region and an unstructured quadrilateral grid region in the semicircle cavities. In the structured quadrilateral grid region, the first cell height near the airfoil is about 2×10^{-5} m, which corresponds to $y^+ \leq 1$ so that the boundary layer flow can be calculated without using wall function, the value of y^+ is shown in Fig. 5. The heights of the cells grow with a factor of 1.045. There are about 1200 grids distributed on the airfoil surface and with high resolution at the leading edge. In the wake region, 220×200 grids are placed in the horizontal and vertical directions, respectively. The total grid number is about 387,000, and the grid number is a little different with the variations of pits size. The global and local illustrations of the grid distribution are shown in Fig. 4.

A series of grids with different cell densities inside the pits have been implemented to study the effects of grid generation schemes on the numerical solutions, as shown in Fig. 6. The initial grid, shown in Fig. 4 was denoted as G1, is considered as the baseline grid, which has 15 nodes at the semicircle and with unstructured quadrilateral grids generation scheme in the pitting cavity. On the basis of G1, a denser grid, G2, with 23 nodes at the semicircle was created with the unstructured quadrilateral cells method. The grids G3, G4, and G5 were created with unstructured triangular schemes, and the nodes at the semicircle are 10, 15, and 20, respectively.

3.1.3 Turbulence Model. The turbulent flow around the airfoil is considered to be separated flow with strong adverse pressure gradient, and the instability in the flow is easily causing transition from laminar to turbulent [23,24]. Thus, to numerical study of the

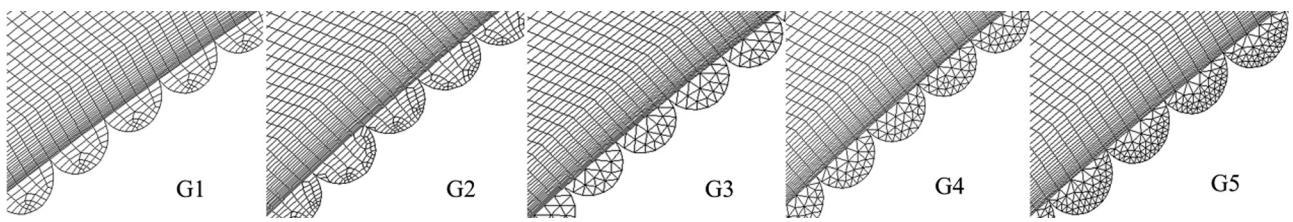

Fig. 6 Grid generation schemes inside the pits

Table 2 The value of C_l/C_d obtained using various grid schemes

	$\alpha = 4.1$ deg		$\alpha = 8.2$ deg		$\alpha = 10.1$ deg	
	C_l/C_d	Difference (%)	C_l/C_d	Difference (%)	C_l/C_d	Difference (%)
G1	32.0412	—	33.6788	—	28.6109	—
G2	31.8819	0.50	33.9551	0.82	28.2169	1.38
G3	31.7325	0.96	34.1396	1.37	28.0859	1.84
G4	31.8180	0.70	33.3223	1.06	28.1466	1.62
G5	31.6848	1.11	33.0211	1.95	27.7282	3.09

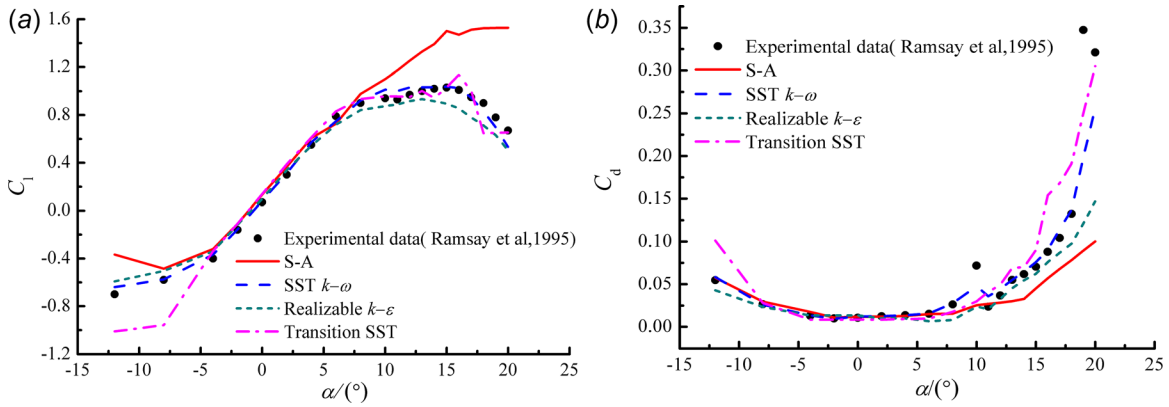

Fig. 7 Lift and drag coefficients versus α for noneroded airfoil at $Re = 1.0 \times 10^6$: (*a*) lift coefficient and (*b*) drag coefficient

aerodynamic characteristics of the pitting eroded airfoil, four turbulence models, i.e., shear stress transport (SST) k–ω model, transition SST model, realizable k–ε model, and S–A model, were adopted to compute the aerodynamics of smooth S809 airfoil and results are compared to the experimental data [25]. These models have been widely applied in wind engineering with promising results for two-dimensional separated flow [17,26,27], and the details of which can be referred to previous publications [24,28].

3.2 Numerical Validation

3.2.1 Grid Sensitivity Studies. The computed results of C_l/C_d obtained using grid G1–G5 are shown in Table 2. G1 is the baseline grid, and the differences among other girds and G1 are presented in Table 2. In general, it can be seen that the differences of all five investigated grids are small, the maximum of which is 3.09% and the minimum is only 0.5%. For the grids G1 and G2, the cells inside the pits are quadrilateral meshes, and the predicted aerodynamics are consistent with each other; however, the cells of G1 are better distributed than G2, and which also show a better convergence. For the grids G3–G5, the grid generation schemes are unstructured quadrilateral meshes, and the result of G4 presents the best agreement with G1, which also has well distributed cells but the convergence is a little worse than G1. Therefore, we take the view that the predicted results obtained using G1 are acceptable and thus the results obtained from the grids generation scheme of G1 are presented in the following part of this paper.

3.2.2 Turbulence Model Studies. Figure 7 presents the computed aerodynamic coefficients of the airfoil with different turbulence models, i.e., SST k–ω, transition SST, realizable k–ε and S–A model, as well as experimental data of Ramsay et al. [25] at the Reynolds number of 1.0×10^6. In Fig. 7(*a*), it is observed that the SST k–ω model yields the most accurate prediction. It is able to capture the peak lift at $\alpha = 15$ deg and match the experimental curve very well for all investigated angles of attack except a little overestimated around the angle of attack 10 deg. Meanwhile, the predicted drag coefficient by the SST k–ω model also agrees well with the experimental data. For the transition SST model, the results agree well with the experiment data from the angles of attack −4.1 deg to 15.2 deg, but they deviate from the experiment results both at high and low angles of attack. In comparison, the realizable k–ε model underestimates the lift coefficient at high angles of attack. The prediction of aerodynamic coefficient by the S–A model deviates significantly from experiment data when the angles of attack are higher than 10 deg.

In order to further evaluate the performance of the SST k–ω turbulence model, the computed pressure coefficients at the angles of attack 8.1 deg and 15 deg are presented in Fig. 8. Excellent agreements with experiment data are also obtained, which indicates that the CFD computation using SST k–ω model could achieve reasonable and accurate results.

In Fig. 7, the results obtained using SST k–ω and transition SST models present better agreements with the experiment measurements than the other two turbulence models. However, the solutions were conducted with smooth airfoil. To examine the predictive ability of the mentioned two turbulence models on the flow field and aerodynamic characteristics of pitting eroded airfoil, a series of simulations were studied, and results were illustrated in Figs. 9 and 10. It is observed in Fig. 9 that the flow fields are nearly the same, and the size of the reversed flow regions presents little difference. Meanwhile, the pressure coefficients overlap with each other except for a protuberance appeared around the region of 55%c of the pressure surface obtained with the transition SST model. Research on other angles of attack showed that the protuberances are existed and become more severe at high angles of attack. In addition, the computation time of the solutions with transition SST is about 1.6 times of that with SST k–ω model at the same conditions. From the above, SST k–ω

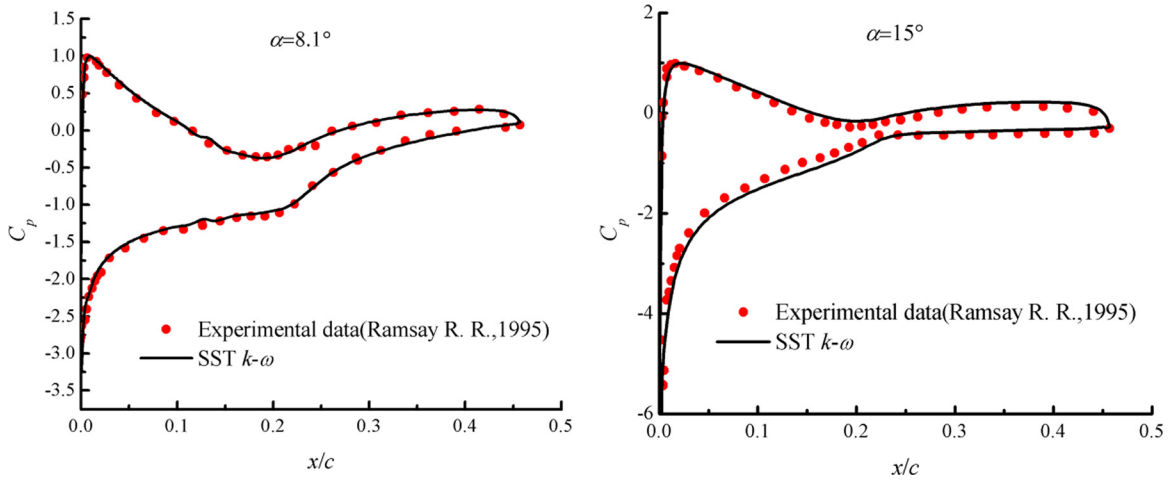

Fig. 8 Pressure coefficient obtained with SST *k–ω* turbulence model at the angles of attack 8.1 deg and 15 deg

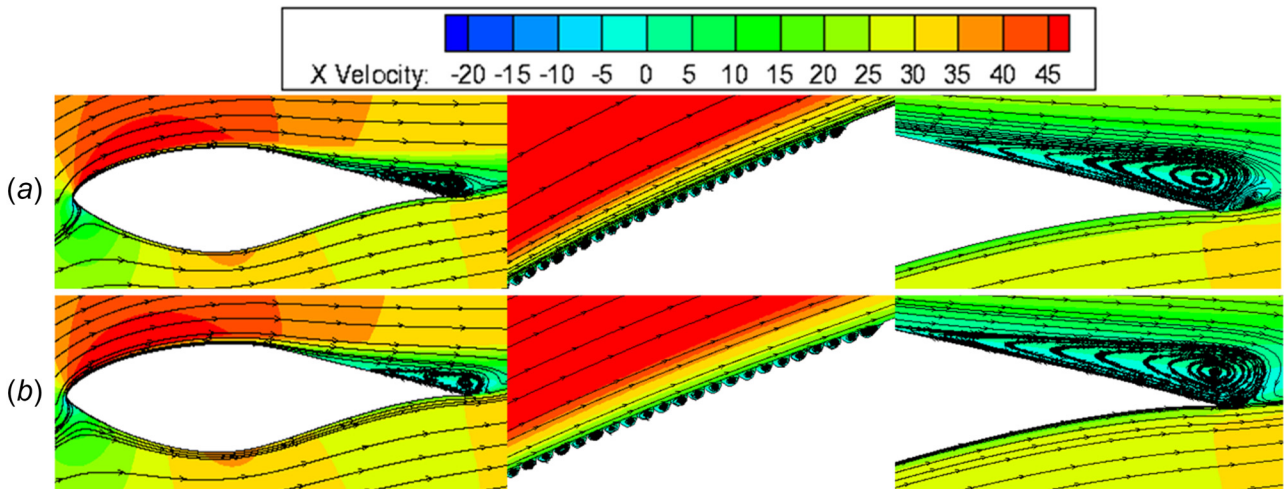

Fig. 9 Streamlines and velocity contours for the pitting eroded airfoil obtained with SST *k–ω* and transitional SST turbulence model. From left to right: flow around the airfoil, flow near the pits at the suction surface, and flow around the tailing edge: (*a*) SST *k–ω* model and (*b*) transition SST model.

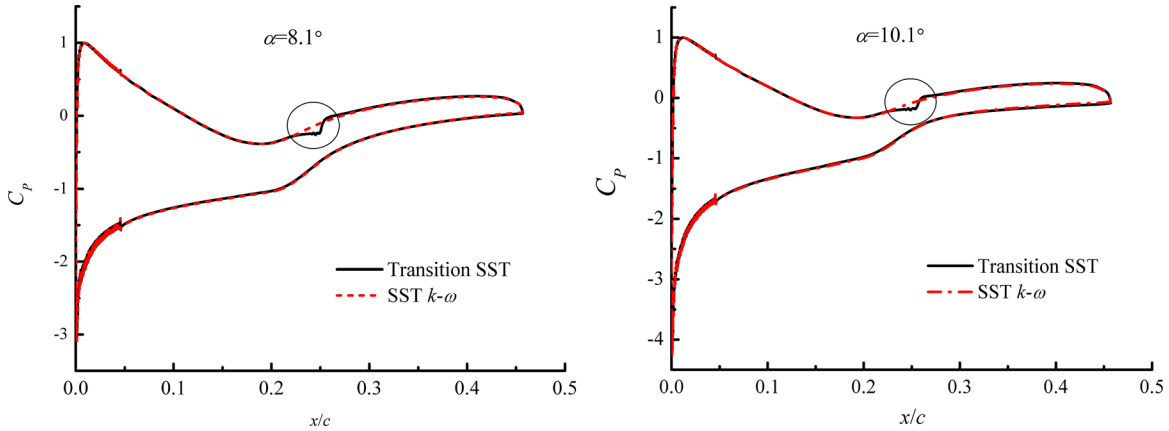

Fig. 10 Pressure coefficients obtained with SST *k–ω* and transitional SST turbulence model at the angles of attack 8.1 deg and 10.1 deg

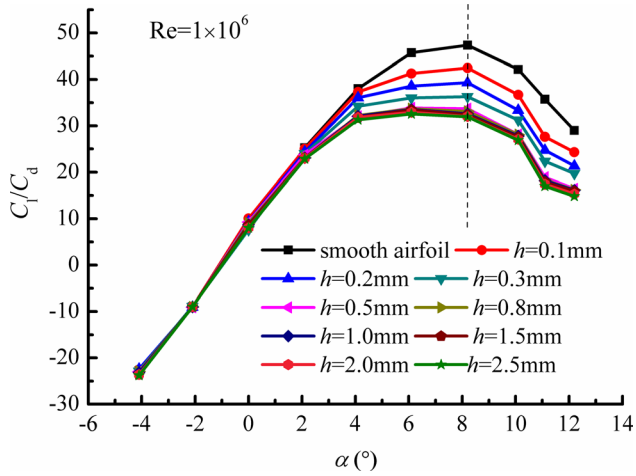

Fig. 11 The value of C_l/C_d versus α for airfoil with various pitting erosion depths

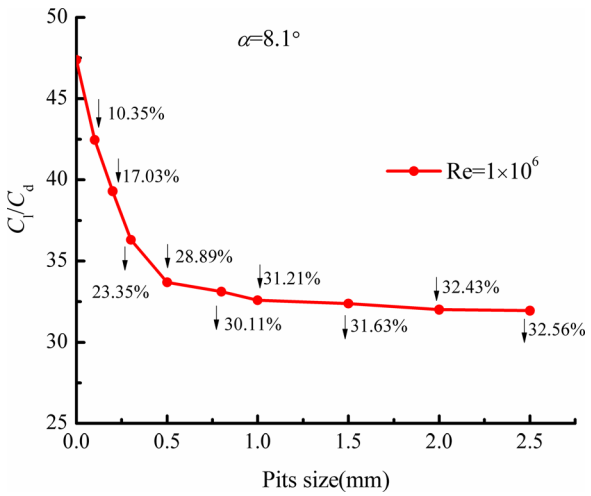

Fig. 12 The relative decrease of C_l/C_d for airfoil with a growing pits size

model can get a good simulation results and with shorter computation time, which is suitable for solving the Reynolds-averaged Navier–Stokes for pitting eroded airfoils in the present study.

4 Results and Analysis

4.1 Aerodynamic Performances With Various Erosion Depths. In order to investigate the effect of pitting erosion depth on the aerodynamic performances of S809 airfoil, the flow over an airfoil with pits distributed closely at the upper and lower surface of the leading edge region ($x/c = 10\%$) has been computed. The pits depths are ranging from 0.1 to 2.5 mm, and their corresponding dimensionless h/c are presented in Table 1. The computed ratio of lift and drag coefficients (C_l/C_d) for airfoils with various pits depths at the Reynolds number of 1×10^6 are shown in Fig. 11, and the relative decrease of C_l/C_d with the increase of pitting erosion depth at the angle of attack 8.1 deg can be seen in Fig. 12.

Lift-to-drag ratio is an important parameter for airfoil design, and the aim is to obtain the maximum C_l/C_d as much as possible. As can be seen in Fig. 11, with the increase of the angle of attack, the value of C_l/C_d grows first and then drops when the angle of attack is greater than 8.1 deg, and 8.1 deg presents the optimal aerodynamic characteristics for the investigated airfoil. The C_l/C_d curves for various pitting erosion depths overlap with each other until the angle of attack reaches 2.1 deg, which demonstrates that pitting erosion has little influence on the aerodynamics of the airfoil at lower angles of attack. Then, with the increase of angle of attack, the effects become intense and reach to the maximum at $\alpha = 8.1$ deg. Meanwhile, the C_l/C_d for airfoils with pits depth greater than or equal to 0.5 mm present little differences, which illustrates that 0.5 mm is a dominant erosion depth for pitting erosion of S809 airfoil. The relative decrease of C_l/C_d for airfoils with different pitting erosion depths presented in Fig. 12 also proves this result. The decrease of C_l/C_d is 28.89% for airfoil with pitting erosion depth of 0.5 mm, and which is just 32.56% when the pits depth is 2.5 mm.

In Fig. 13, the effects of pits size on the aerodynamics of the airfoil were calculated at the Reynolds number of 0.75×10^6, 1.0×10^6 and 1.5×10^6 at the angle of attack 8.1 deg. It is obviously seen that the lift and drag coefficients change rapidly when the erosion depth is smaller than 0.5 mm, while they reach almost plateau when the erosion depth is greater than 0.5 mm. The trends are similar at three Reynolds numbers, which demonstrates that the pits depth of 0.5 mm ($h = 0.0005c$) is a critical value and beyond which the aerodynamic performances of the airfoil are insensitive to the pitting erosion depth. For all cases, the maximum lift decrease is 6.2% and the maximum drag increase is 43.1%, which demonstrates that pitting erosion has great influence on the aerodynamic characteristics of S809 airfoil.

Figure 14 presents the flow field contours around the airfoil with various pitting erosion depths at the Reynolds number of

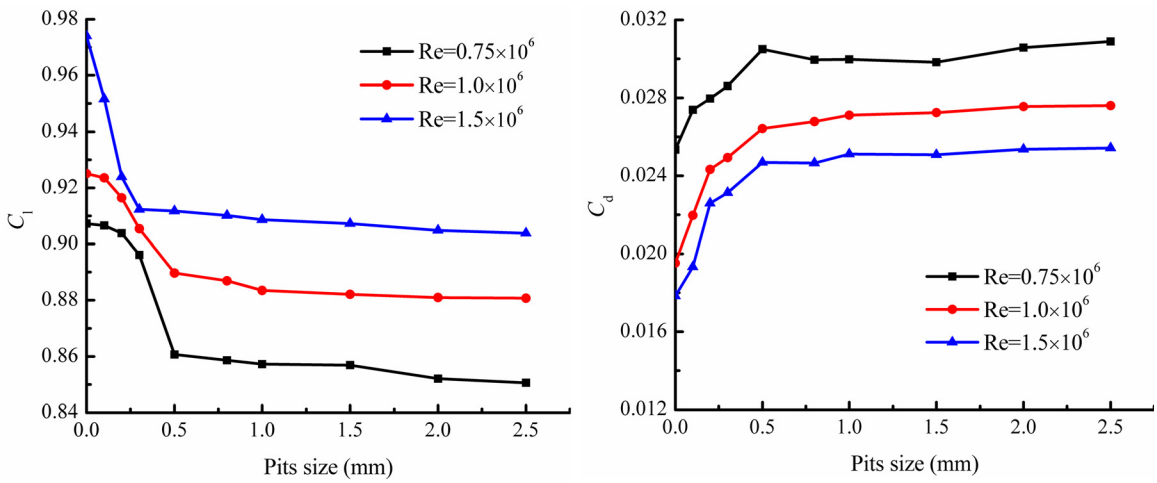

Fig. 13 Computed lift and drag coefficients with different erosion depth

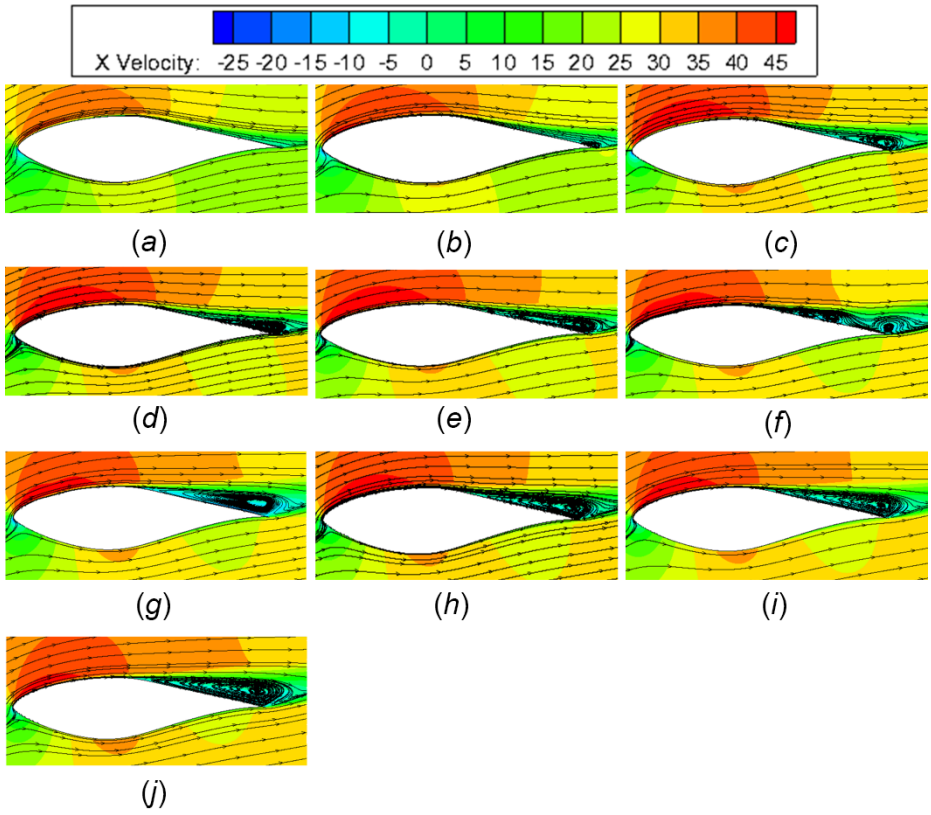

Fig. 14 Streamlines and velocity contours for S809 airfoils with various pitting erosion depth at Re = 1.0×10^6 ($\alpha = 8.1$ deg): (*a*) smooth airfoil, (*b*) $h = 0.1$ mm, (*c*) $h = 0.2$ mm, (*d*) $h = 0.3$ mm, (*e*) $h = 0.5$ mm, (*f*) $h = 0.8$ mm, (*g*) $h = 1.0$ mm, (*h*) $h = 1.5$ mm, (*i*) $h = 2.0$ mm, and (*j*) $h = 2.5$ mm

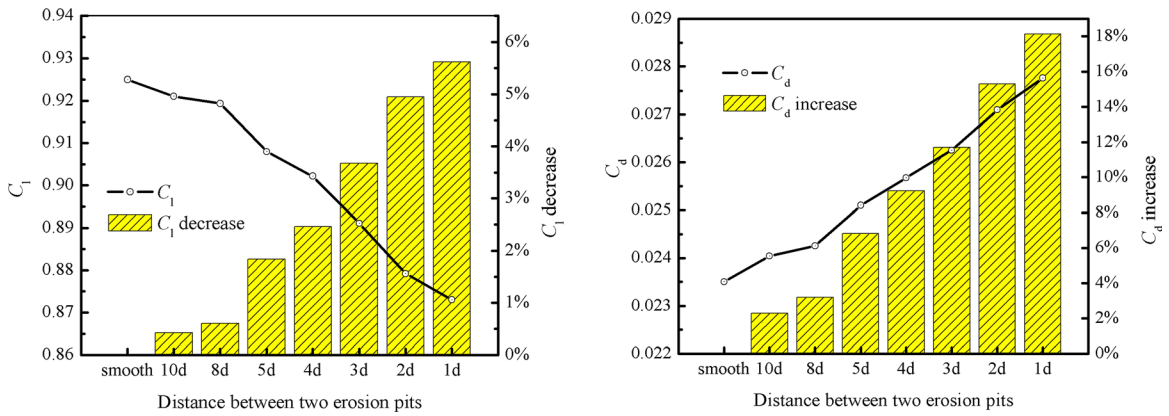

Fig. 15 Lift and drag coefficients of airfoils with various pits densities

1.0×10^6. It can be seen that the flow is fully attached to the airfoil when the erosion is not imposed, and a small region of separated flow can be observed near the tailing edge of the suction surface even if the airfoil pitting eroded with a depth of 0.1 mm. This reversed flow region increases gradually with the increase of erosion depth, and can span over one-third of the suction surface of the airfoil when the erosion depth is 0.5 mm. For airfoils with the erosion depth greater than 0.5 mm, the flow separation region grows a little and can span over nearly half of the suction surface; however, the growth is small and its influence can be neglected when compared to the airfoil with a pitting erosion depth of 0.5 mm. The separated flow gives rise to the pressure drag on the airfoil, which causes the lift decrease and drags increase, and finally affects the aerodynamic performance of the airfoil as mentioned before.

4.2 Aerodynamic Performances With Different Pits Densities. It has been proposed that surface roughness density plays great role in the performance degradation of an airfoil [29]. In order to explore the effects of pits erosion density, the distance between two semicircle cavities is denoted as a reference value for pits density in the present study. The erosion pits were distributed at the leading edge 10%*c* region of the airfoil with various densities, i.e., $l = 1d$, $2d$, $3d$, $4d$, $5d$, $8d$ and $10d$. Here, l is the distance between two erosion pits and d is the diameter of semicircle

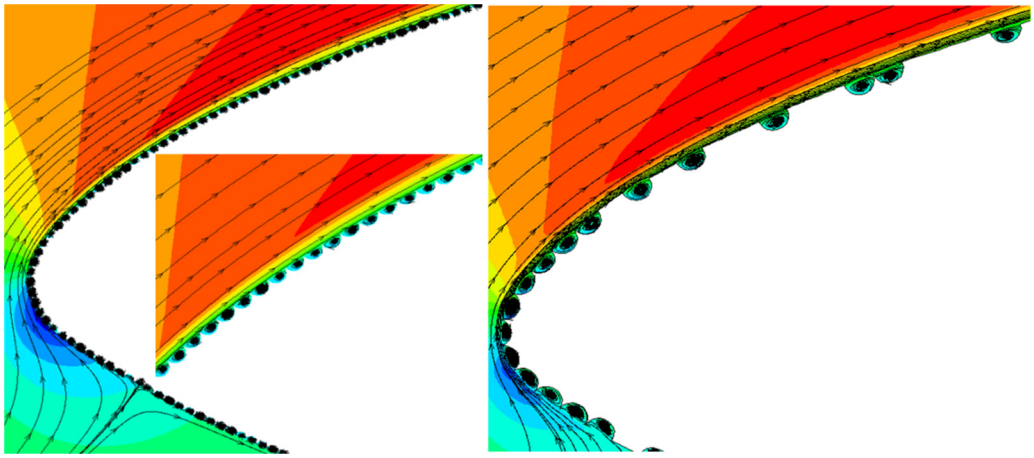

Fig. 16 The streamlines around the pitting eroded leading edge (*a*). The leading edge with equally distributed erosion pits. (*b*) The leading edge with random distributed pits.

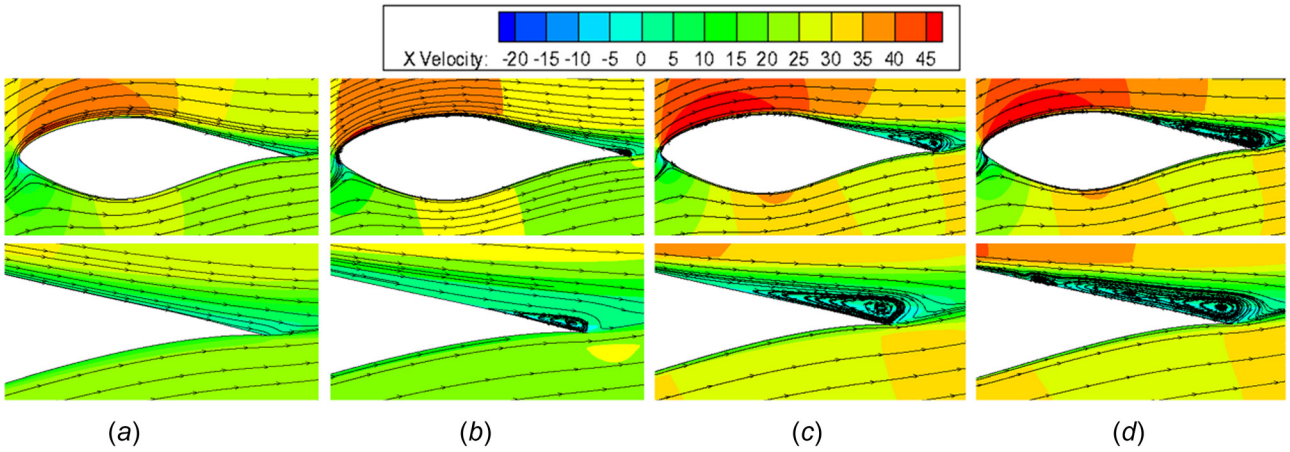

Fig. 17 Streamlines and velocity magnitude contours for airfoils with various pitting erosion densities. (*a*) Smooth airfoil. (*b*) The distance between two erosion pits is 8*d*. (*c*) The distance between two erosion pits is 4*d*. (*d*) The distance between two erosion pits is 1*d*.

cavity. The study was conducted on the airfoil with the pits depth of 0.5 mm at the angle of attack 8.1 deg.

The computed aerodynamic coefficients are shown in Fig. 15. As can be seen that with the increase of pits density, the lift decreases and drag increases. When compared to smooth airfoil, the lift decreases 0.6% and drag increases about 3% for airfoil eroded with a pits density of $l = 8d$, while the lift decreases 1.84% and drag increases about 6.8% for airfoil covered with a distance between two pits of 5*d*. The lift drops around 5.5% when the pits are arranged densely ($l = 1d$), and the drag increases about 18%, which is the most influence case. Therefore, the aerodynamic performance of the airfoil is very sensitive to pits density, and the drag coefficient is more susceptible. When the distance between two pits is greater than 8*d*, the pitting erosion has a relatively little effect on the aerodynamic performance of the airfoil.

It can be seen from Fig. 16 that there are small flow swirls inside the erosion cavity, and no flow separations can be observed on the surface of the airfoil, whether the airfoil eroded with closely distributed pits (Fig. 16(*a*)) or not (Fig. 16(*b*)). Therefore, the more the erosion pits on the surface of the airfoil, the more flow swirls and more energy cost, which cause the drag increase and lift decrease. Figure 17 presents the flow field contours around the airfoils with the erosion pits distances of 8*d*, 4*d*, and 1*d*, and compared with that of smooth airfoil. It can be seen that there is no flow separation around the smooth airfoil, while a small tailing edge separation region can be observed when the leading edge is covered by the erosion pits with a distance of $l = 8d$. As the pitting erosion density increases, the size of flow separation region grows, which gives rise to lift coefficient decrease and drag coefficient increase.

4.3 Aerodynamic Performance With Different Pits Areas. To investigate the effect of pits erosion area on the aerodynamic performance of the airfoil, computations were carried out at the angle of attack 8.1 deg and Reynolds number of 1.0×10^6. The airfoil is covered by the closely arranged erosion pits with a depth of 0.5 mm, and the considered erosion areas (x/c) are 1%, 2%, 3%, 4%, 5%, 8%, 10%, and 13% in the study, and results are presented in Fig. 18. It can be seen that with the increase of pitting erosion area, the lift coefficient decreases and the drag coefficient increases. For airfoil with an erosion area of 5%*c*, the lift drops about 9.2% while the drag coefficient increases about 47.7% compared with smooth airfoil. When the erosion area is greater than 5%*c*, the lift and drag vary much more slowly. For airfoil with an erosion area of 13%*c*, the lift coefficient decreases about 1.6% and drag coefficient increases about 7.9% when compared to 5%*c* erosion length case. Figure 19 presents a detailed pressure coefficient for airfoils with various pitting erosion areas, it can be observed that the pressure coefficient of airfoil with the erosion

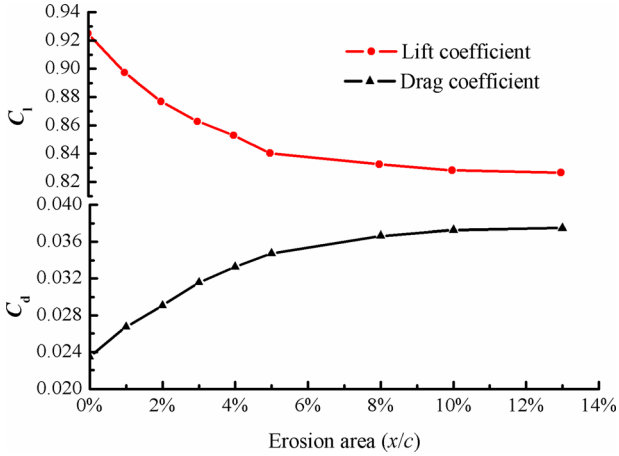

Fig. 18 Lift and drag coefficients under different pit erosion areas

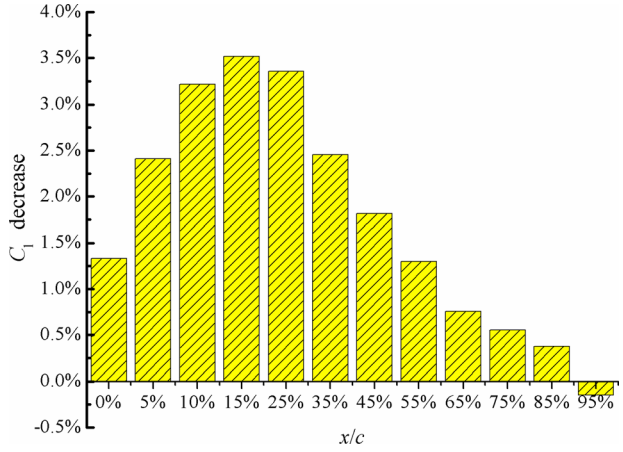

Fig. 20 The lift decrease for airfoil with pitting erosion at various locations

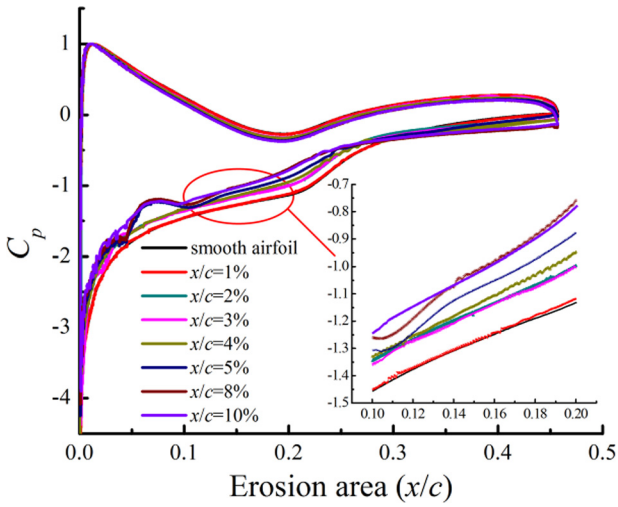

Fig. 19 Pressure coefficients for the airfoil with various pitting erosion areas

area of 1%c is very close to that of smooth airfoil, which indicates that small area pitting erosion has little influence on the aerodynamic characteristics of the airfoil. As the erosion areas increase, the pressure coefficients show differences with each other at the suction surface. For airfoils with the erosion area greater than 5%c, the pressure coefficients almost overlap with each other, which indicates that the aerodynamics change little when the pitting erosion area is greater than 5%c, and the results are in accordance with the lift and drag coefficients illustrated in Fig. 18. Therefore, it can be concluded that 5%c is a critical erosion area for airfoil and beyond which the aerodynamic coefficient changes slightly.

4.4 Aerodynamics Performances With Different Erosion Locations. To investigate the effects of pitting erosion locations on the aerodynamic performance of the airfoil, computations for airfoils with pits belts located at different positions were conducted at the angle of attack 8.1 deg and Reynolds number of 10^6. The erosion belt has a width of 2%c and the pits depth is 0.5 mm, which was located at the position of $x/c = 0\%$, 5%, 10%, 15%, 25%, 35%, 45%, 55%, 65%, 75%, 85%, and 95% of the suction surface of the airfoil, respectively. The results showed that the greatest lift reduction occurs at the location of $x/c = 15\%$ (in Fig. 20), where the lift decreases about 3.52% and drag increases 15.2%. Consequently, the location of $x/c = 15\%$ is regarded as the most influential area to affect the aerodynamic properties of the airfoil. In addition, the pitting erosion has a more evident influence when it is located in the first half of the airfoil. The reason is that pitting erosion near the leading edge can drain a large amount of momentum from the turbulent boundary layer for the local velocities are much higher than other region of the airfoil, reducing that available for pressure recovery. As the erosion belt moves to the tail edge gradually, the surface velocities become much lower and the boundary layer much thicker such that the erosion results in little momentum loss and has little impact on the aerodynamic performance. It has also been discovered that surface roughness at the thickest area of the airfoil is more easily to evocate variations of the aerodynamic coefficients of the airfoil [30].

4.5 Path Coefficient Analysis. Path coefficient analysis developed by Wright [31] is a useful method in analyzing the relationship between independent and dependent variables, and partitioning the direct effects of one independent variable on the dependent variable and the indirect effects of one independent variable on the dependent variable through other independent variables. Here, this method was adopted to find out the dominant parameter of pitting erosion through comparing the direct effects of the previously mentioned parameters on the aerodynamics of the airfoil, and obtain the relative importance of independent variable by analyzing direct effects and indirect effects of these pitting erosion influence parameters.

The path analysis was conducted at the angle of attack 8.1 deg, since the influence of angle of attack on the aerodynamics is much greater than that of pitting erosion, so the variation of the angle of attack was not considered in this study. Lift coefficient of the airfoil was taken as the performance assessment indicator, the dependent variable (y), and the influence parameters, pits depth (x_1), pits area (x_2), pits density (x_3), pits locations (x_4), and Reynolds number (x_5) were taken as the independent variables (x_i). The correlation coefficient ($r_{x_i y}$) between lift coefficient (y) and one impact factor (x_i) is decomposed into direct effects (unidirectional pathways, P_{yx_i}) and indirect effects through alternate pathways (pathway, (P_{yx_j}) $\times$ correlation coefficients ($r_{x_i x_j}$)). Here, $r_{x_i y}$ is the correlation coefficient between independent variable (x_i) and dependent variable (y), $r_{x_i x_j}$ is the correlation coefficient between two independent variables (x_i, x_j), P_{yx_i} is the direct effect of independent variable (x_i) on dependent variable (y), $P_{yx_j} r_{x_i x_j}$ is the indirect effect of independent variable (x_i) on dependent variable (y) through another independent variable (x_j). The path coefficients are obtained by analyzing 105 groups of computational results based on various pitting erosion impact factors using the software of SAS [32], and the fundamental of the analysis is to

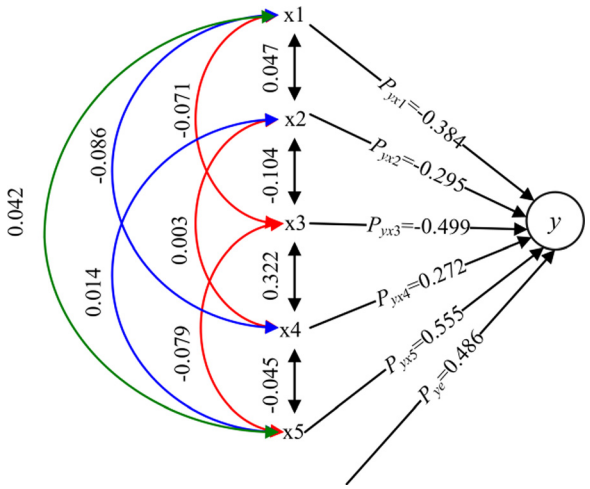

Fig. 21 A path diagram and coefficients of pitting erosion parameters

Table 3 Path coefficient analysis of C_l and indirect effects involved in pitting erosion

			Indirect effects $P_{yx_j} \cdot r_{x_i x_j}$				
Impact factors	$r_{x_i y}$	P_{yx_i}	$x_1 \to y$	$x_2 \to y$	$x_3 \to y$	$x_4 \to y$	$x_5 \to y$
x_1	−0.363	−0.384		−0.014	0.009	−0.023	−0.202
x_2	0.256	−0.295	−0.019		0.052	0.001	0.008
x_3	−0.397	−0.499	0.027	0.031		0.088	−0.044
x_4	0.120	0.272	0.033	−0.001	−0.161		−0.025
x_5	0.567	0.555	−0.016	−0.004	0.039	−0.012	

solve the simultaneous equations through the least-squares method [33].

The interrelationship coefficients among pits depth, area, density, location, Reynolds number, and lift coefficient are shown in Fig. 21. The double-arrowed lines indicate the mutual effects between two independent variables by correlation coefficients ($r_{x_i x_j}$), and single-arrowed lines represent the direct effects by path coefficients (P_{yx_j}). P_{ye} is the residual term, which mainly refers to the pitting erosion impact factors not considered in the analysis. As can be seen in Fig. 21, Reynolds number has the greatest direct effect coefficient (0.555), followed by that of pitting erosion density (−0.499), which indicates that Reynolds number and pits density are the two predominant factors on the aerodynamics of airfoil for pitting erosion. The pitting erosion location has the smallest influence coefficient among the considered parameters. It is also worth to be noted that the value of the residual factors (0.486) is very large, which indicates that some important factors should be out of consideration, here maybe the angle of attack, an important impact factor. In addition, the correlation coefficients ($r_{x_i x_j}$) between two independent variables are quite small, which indicates that the parameters are relatively independent with each other.

Estimations of the direct and indirect path coefficients among the considered parameters are presented in Table 3. It can be seen that all the indirect effects are relative small, in which the largest one is 0.202 and all of them are smaller than direct effects shown in Fig. 21. This illustrated that the influence of one pitting erosion factors via other parameters on the aerodynamics is small, i.e., the effect of pitting erosion size on the lift coefficient of the airfoil is just 0.009 via the pits density, and the influence is much less than the direct effects. The results showed that pits depth, area, density, and location should be independent, and have little correlations with each other.

5 Conclusions

In this work, a computational study on the effect of leading edge pitting erosion on the aerodynamic performances of a S809 airfoil is conducted through a well-validated CFD simulation. A new pitting erosion model is proposed and semicircle cavities are used to represent the erosion pits. Several erosion parameters, such as pits depth, pits area, pits density, and pits location, are adopted to investigate their influences on the aerodynamic characteristics of the airfoil. In addition, interrelationships among these factors and the lift coefficient of the airfoil are determined by a path coefficient analysis.

The main conclusions are as follows:

(a) The effect of pitting erosion depth on the aerodynamics of the airfoil grows first and then drops a little, the pits depth has the greatest influence at the angle of attack 8.1 deg, while having little influence when the angle of attack is smaller than 2.1 deg. The aerodynamic performance of the S809 airfoil is more significantly influenced by pitting erosion when the pits depth is less than 0.5 mm.

(b) When the distance between two erosion pits is less than eight times of the pits diameter, the lift coefficient decreases and drag coefficient increases significantly. Higher erosion density will induce more severe influence on the aerodynamics of the airfoil. The lift drops sharply if the first 5%c of the airfoil is eroded, while it reaches nearly constant when the erosion area spans to 10%c of the suction surface.

(c) The aerodynamic coefficients are mostly affected when the erosion area is located at the first 15% of the airfoil in chordwise. Moreover, the lift and drag of airfoil are more sensitive to pits erosion location of the first half than the last half of the airfoil.

(d) The path coefficient analysis shows that the direct effects of pitting erosion parameters on the lift coefficient are larger than indirect effects, and the considered impact factors are highly independent. For all the considered erosion parameters, the Reynolds number is the most influential, followed by pits density, pits depth, pits area, and pits location.

The erosion features are complex and different for wind turbine blade, and the present work is just a first attempt to model the early stage of leading edge erosion. Studies on other kinds of erosion model much closer to real conditions or three-dimensional erosion are of great importance and interests need to be investigated in future.

Acknowledgment

The authors would like to acknowledge the financial support from the National Natural Science Foundation of China (Nos. 11490553, 11502185, and 11362010), the Innovative Research Group of the National Natural Science Foundation of China (No. 11120202), and the Natural Science Foundation of Gansu Province (No. 1308RJYA066) and Ramsay et al. from National Renewable Energy Laboratory for the details and data of the previous work.

References

[1] Zhang, S., Dam-Johansen, K., Nørkjær, S., Bernad, P. L., and Kiil, S., 2013, "Erosion of Wind Turbine Blade Coatings—Design and Analysis of Jet-Based Laboratory Equipment for Performance Evaluation," Prog. Org. Coat., **78**, pp. 103–115.

[2] Siddons, C., Macleod, C., Yang, L., and Stack, M., 2015, "An Experimental Approach to Analysing Rain Droplet Impingement on Wind Turbine Blade Materials," EWEA Annual Event, Paris, France, Nov. 17–20.

[3] Zhang, S., Dam-Johansen, K., Bernad, P. L., and Kiil, S., 2015, "Rain Erosion of Wind Turbine Blade Coatings Using Discrete Water Jets: Effects of Water Cushioning, Substrate Geometry, Impact Distance, and Coating Properties," Wear, **328–329**, pp. 140–148.

[4] Keegan, M. H., Nash, D., and Stack, M., 2013, "On Erosion Issues Associated With the Leading Edge of Wind Turbine Blades," J. Phys. D, **46**(38), p. 383001.
[5] Chinmay, S., 2012, "Turbine Blade Erosion and the Use of Wind Protection Tape," M.S. thesis, University of Illinois, Champaign, IL.
[6] Sareen, A., Sapre, C. A., and Selig, M. S., 2014, "Effects of Leading Edge Erosion on Wind Turbine Blade Performance," Wind Energy, **17**(10), pp. 1531–1542.
[7] Powell, S., 2011, "3M Wind Blade Protection Coating W4600," Industrial Marketing Presentation, http://www.3M.com. or http://www.pressebox.com/attachment/404803/Wind_Tape_Example_mittel. jpg.
[8] Wang, Y., 2012, "The Status Quo of Wind Turbine Blades Development in China," Wind Energy Resour., **2**, pp. 11–14.
[9] Ehrmann, R. S., White, E. B., Maniaci, D. C., Chow, R., Langel, C. M., and Van Dam, C. P., 2013, "Realistic Leading-Edge Roughness Effects on Airfoil Performance," AIAA Paper No. 2013-2800.
[10] Lu, J., Mu, S., and Li, Q., 2015, "Progress on Leading Edge Protection Technology of Wind Turbine Blades," Fiber Reinf. Plast./Compos., **7**, pp. 91–95.
[11] White, E. B., Kutz, D., Freels, J., Hidore, J. P., Grife, R., Sun, Y. P., and Chao, D., 2011, "Leading-Edge Roughness Effects on 633-418 Airfoil Performance," AIAA Paper No. 2011-352.
[12] McGowan, J. G., and Connors, S. R., 2000, "Windpower: A Turn of the Century Review," Annu. Rev. Energy Environ., **25**(1), pp. 147–197.
[13] Standish, K., Rimmington, P., Laursen, J., Paulsen, H. N., and Nielsen, D., 2010, "Computational Prediction of Airfoil Roughness Sensitivity," AIAA Paper No. 2010-460.
[14] Sareen, A., Sapre, C., and Selig, M., 2012, "Effects of Leading-Edge Protection Tape on Wind Turbine Blade Performance," Wind Eng., **36**(5), pp. 525–534.
[15] Slot, H., Gelinck, E., Rentrop, C., and Van der Heide, E., 2015, "Leading Edge Erosion of Coated Wind Turbine Blades: Review of Coating Life Models," Renewable Energy, **80**, pp. 837–848.
[16] Amirzadeh, B., Louhghalam, A., Raessi, M., and Tootkaboni, M., 2017, "A Computational Framework for the Analysis of Rain-Induced Erosion in Wind Turbine Blades—Part II: Drop Impact-Induced Stresses and Blade Coating Fatigue Life," J. Wind Eng. Ind. Aerodyn., **163**, pp. 44–54.
[17] Gharali, K., and Johnson, D. A., 2012, "Numerical Modeling of an S809 Airfoil Under Dynamic Stall, Erosion and High Reduced Frequencies," Appl. Energy, **93**, pp. 45–52.
[18] Wang, Y., Zheng, X., and Hu, R., 2016, "Effects of Leading Edge Defect on the Aerodynamic and Flow Characteristics of an S809 Airfoil," PLoS One, **11**(9), p. e0163443.
[19] Gaudern, N., 2014, "A Practical Study of the Aerodynamic Impact of Wind Turbine Blade Leading Edge Erosion," J. Phys., **524**(1), p. 012031.
[20] Rempel, L., 2012, "Rotor Blade Leading Edge Erosion-Real Life Experiences," Wind Syst. Mag., **10**, pp. 22–24.
[21] Wang, Y. L., 2009, "The Process of the Erosion of a Rigid Wind Turbine Blade," Shenyang Lvxinxin New Wind Energy Equipment Maintenance Co., Shenyang, China, accessed Aug. 24, 2017, http://www.flfdwh.com/view.asp?id=26
[22] ANSYS, 2010, "ANSYS FLUENT 13.0 (Theory Guide)," ANSYS, Inc., Canonsburg, PA.
[23] Anderson, J. D., 2010, *Fundamentals of Aerodynamics*, McGraw-Hill Education, New York.
[24] Wang, Y., Hu, R. F., and Wang, P., 2017, "Research on the Aerodynamic and Flow Field Characteristics of S809 Airfoil Based on the Leading Edge Erosion Modeling," Acta Energ. Sol. Sin., **38**(37), pp. 605–613.
[25] Ramsay, R. R., Hoffmann, M. J., and Gregorek, G. M., 1995, "Effects of Grit Roughness and Pitch Oscillations on the S809 Airfoil," National Renewable Energy Laboratory, Golden, CO, Report No. NREL/TP-442-7817.
[26] Guerri, O., Bouhadef, K., and Harhad, A., 2006, "Turbulent Flow Simulation of the NREL S809 Airfoil," Wind Eng., **30**(4), pp. 287–301.
[27] Wang, S., Ingham, D. B., Ma, L., Pourkashanian, M., and Tao, Z., 2012, "Turbulence Modeling of Deep Dynamic Stall at Relatively Low Reynolds Number," J. Fluids Struct., **33**, pp. 191–209.
[28] Menter, F., Kuntz, M., and Langtry, R., 2003, "Ten Years of Industrial Experience With the SST Turbulence Model," Turbul., Heat Mass Transfer, **4**(1), epub.
[29] Huebsch, W. W., and Rothmayer, A. P., 2004, "Numerical Prediction of Unsteady Vortex Shedding for Large Leading-Edge Roughness," Comput. Fluids, **33**(3), pp. 405–434.
[30] Ren, N., and Ou, J., 2009, "Dust Effect on the Performance of Wind Turbine Airfoils," J. Electromagn. Anal. Appl., **1**(2), pp. 102–107.
[31] Wright, S., 1921, "Correlation and Causation," J. Agric. Res., **20**(7), pp. 557–585.
[32] SAS Institute, 1985, *SAS User's Guide: Statistics*, SAS Institute, Cary, NC.
[33] Dewey, D. R., and Lu, K., 1959, "A Correlation and Path-Coefficient Analysis of Components of Crested Wheatgrass Seed Production," Agron. J., **51**(9), pp. 515–518.